Accepted by the Journal of ASTM International (2009)

# A Materials Science-Based Approach to Characterizing Fire Resistive Materials

Dale P. Bentz[1]
Christopher C. White
Kuldeep R. Prasad
Daniel R. Flynn
Donald L. Hunston
Kar Tean Tan

Building and Fire Research Laboratory
National Institute of Standards and Technology
Gaithersburg, MD 20899-8615 USA

## Abstract

While ASTM E119-07a is commonly employed to establish a fire rating for a fire resistive material (FRM)/steel assembly, the test method provides little quantitative information on either the thermophysical or adhesion properties of the FRM, beyond indicating that they are sufficient to achieve the measured rating. As part of the Building and Fire Research Laboratory (BFRL) Structural Performance Under Multi-hazards program, a materials science-based approach is being applied to develop new methodologies and test methods for characterizing these complex dynamic materials. These quantitative characterizations can then be used as inputs to thermal/mechanical performance models and also for obtaining a better understanding of how these materials perform their intended role and how they could be improved. Thermophysical properties that must be characterized as a function of temperature include density, heat capacity, thermal conductivity, and heats of reactions and phase changes. For example, for high temperature thermal conductivity, a new measurement technique based on the use of a slug calorimeter has been developed and standardized in the ASTM E37 Thermal Measurements committee. In addition to adequate thermophysical properties, adhesion properties are critical to ensure that the FRM continues to protect its substrate during a fire exposure. Research on developing new test methods for both laboratory and field evaluations of adhesion will be presented. Like thermal properties, adhesion has also been observed to be strongly influenced by exposure to elevated temperatures. Finally, capabilities developed at NIST to obtain quantitative descriptions of the three-dimensional microstructures of FRMs and relate them to thermal properties such as thermal conductivity will be demonstrated. Much of this research has been completed as part of the ongoing NIST/industry consortium on "Performance Assessment and Optimization of Fire Resistive Materials."

Keywords: Adhesion; Building technology; Fire resistive material; Materials science; Modeling; Thermal conductivity; X-ray microtomography.

[1] Presenting author: E-mail: dale.bentz@nist.gov, Phone: (301)975-5865, Fax: (301)990-6891

## Introduction

In recent years, the critical functionality of fire resistive materials in protecting structural steel has been recognized, as highlighted in the World Trade Center (WTC) investigation [1]. These materials are designed to insulate structural steel during a fire exposure, limiting the temperature rise of the steel so that its mechanical properties are preserved for an adequate time to allow for safe evacuation. To fulfill this life safety role properly, these materials must function as appropriate thermal insulators at high temperatures and must also remain in place near the steel surface. Thus, both thermophysical and adhesion properties are paramount and must be well-characterized as a function of temperature to enable predictive modeling and improvement and optimization of these materials. This paper presents a materials science-based approach to characterizing these properties.

## Thermophysical Properties

To model appropriately the thermal response of a steel structure protected by a FRM, detailed knowledge of the FRM's density, heat capacity, and thermal conductivity as a function of temperature and quantification of any endothermic or exothermic reactions and/or phase changes that the FRM may undergo during a high temperature exposure are necessary. Previously, a methodology for obtaining all of these parameters has been presented [2,3]. In the present paper, the emphasis will be on measuring thermal conductivity, as this thermophysical property may change by up to a factor of five or more during a fire exposure. Conversely, for many fire resistive materials, heat capacity is on the order of 1000 J/(kg·K) and may only change by 20 % or less between room temperature and 1000 ºC [2-4]. Density variations with temperature during a fire exposure are also generally less than a factor of two, as most FRMs will lose 10 % to perhaps 30 % of their initial mass during an exposure to 1000 ºC, due to dehydration, decarbonation, and other thermal degradation reactions [2-4].

This paper focuses on test methods for the fundamental characterization of the thermal and adhesion properties of FRMs, and does not address the equally complex issue of utilizing these properties in thermal and mechanical models for performance during an actual fire exposure. It is well recognized that such models may need to not only include thermal properties as a function of temperature (and thus spatial location), but also provide for a dynamic simulation of the reactions, phase changes, and mass transport that occur during a fire exposure, as was implemented by NIST during the WTC investigation [1].

### *Thermal Conductivity*

Recognizing that a new method was needed for evaluating the apparent thermal conductivity of fire resistive materials, a slug calorimeter method originally presented by Fitch [5] was adapted to a rectangular geometry set of twin specimens of FRM [4,6,7]. In 2007 [8], this new method was standardized as ASTM E2584-07 "Standard Practice for Thermal Conductivity of Materials Using a Thermal Capacitance (Slug) Calorimeter." Ongoing efforts include an interlaboratory study with ten participants to establish a multi-laboratory precision statement for the new standard. While the derivation of the solution for thermal conductivity based on measurement of the slug and FRM surface temperatures has been presented previously

for the rectangular geometry [4,6], a similar derivation that has been recently performed for a cylindrical geometry is presented here to demonstrate the necessary heat transfer analysis. A cylindrical geometry may offer advantages when testing intumescent FRMs that expand greatly during a high temperature exposure, particularly if they will be used to protect pipes or other cylindrical conduits in their real world application.

For a cylindrical slug calorimeter, the basic geometry as shown in Fig. 1 consists of a hollow cylinder (annulus) of FRM of outer radius ***b*** surrounding a cylindrical slug (rod) of radius ***a***, well insulated at top and bottom so that heat flow is only in the radial direction. The objective is to derive an expression for the thermal conductivity of the FRM as estimated from the heat flow to the cylindrical steel rod under pseudo steady-state (rate) conditions.

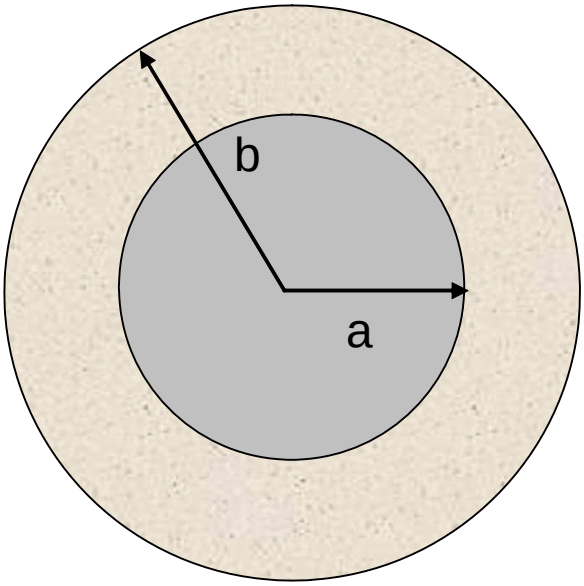


Fig. 1. Schematic of geometry for cylindrical version of the slug calorimeter.

Assuming constant properties (for a small period of time or small temperature change), the temperature, $T$, in the specimen must satisfy:

$$\frac{\partial^2 T}{\partial r^2} + \frac{1}{r}\frac{\partial T}{\partial r} = \frac{1}{\alpha}\frac{\partial T}{\partial t} \tag{1}$$

where:
$r$ = radial distance, m,
$t$ = time, s, and
$\alpha = k/C$ = the thermal diffusivity of the specimen, $m^2/s$, with
$k$ = thermal conductivity, W/(m·K),
$C = \rho c_p$ = volumetric heat capacity, J/($m^3$·K), and
$\rho$ = material density, kg/$m^3$.
For this geometry, the "thermal capacity," $H$, of the cylindrical slug in J/(m·K) is :

$$H = \pi a^2 C_{slug} \tag{2}$$

The heat flow per unit length, $q$, from the specimen into the slug in W/m is:

$$q = -2\pi ak \left.\frac{\partial T}{\partial r}\right|_{r=a} \tag{3}$$

The power absorbed by the slug in W/m is also given by:

$$q = H \left.\frac{\partial T}{\partial t}\right|_{r=a} \tag{4}$$

Thus, the boundary condition at the specimen-slug (radial) interface is:

$$2\pi ak \left.\frac{\partial T}{\partial r}\right|_{r=a} + H \left.\frac{\partial T}{\partial t}\right|_{r=a} = 0 \tag{5}$$

If $F$ is the constant rate at which temperature is changing (positive or negative) in K/s,

$$T(b,t) = Ft \tag{6}$$

an assumed solution takes the form:

$$T(r,t) = A + B\ln\left(\frac{r}{a}\right) + F\left(t + \frac{r^2}{4\alpha}\right) + transient\_terms \tag{7}$$

Since equation (7) must satisfy equations (5) and (6) at times long enough for the transient terms to be neglected, $A$ and $B$ must be selected such that equations (5) and (6) are satisfied in that limiting case.

At $r=b$,

$$T(b,t) = A + B\ln\left(\frac{b}{a}\right) + F\left(t + \frac{b^2}{4\alpha}\right) = Ft \text{, so that}$$

$$A = -B\ln\left(\frac{b}{a}\right) - \frac{Fb^2}{4\alpha} \tag{8}$$

Substituting equation (8) into equation (7) and dropping the transient terms gives:

$$T(r,t) = Ft + B\ln\left(\frac{r}{b}\right) - \frac{F(b^2 - r^2)}{4\alpha} \tag{9}$$

from which the partial derivatives are evaluated to be:

$$\frac{\partial T}{\partial r} = \frac{B}{r} + \frac{Fr}{2\alpha}$$

$$\left.\frac{\partial T}{\partial r}\right|_{r=a} = \frac{B}{a} + \frac{Fa}{2\alpha} \tag{10a}$$

and

$$\frac{\partial T}{\partial t} = F \qquad \text{(at all r)} \tag{10b}$$

Substituting equations (10a) and (10b) into equation (5) gives:

$$2\pi ak\left(\frac{B}{a} + \frac{Fa}{2\alpha}\right) + FH = 0 \qquad \text{from which}$$

$$B = -\frac{F}{2}\left(\frac{a^2}{\alpha} + \frac{H}{\pi k}\right) \quad . \tag{11}$$

Finally, substituting equation (11) into equation (9) yields:

$$T(r,t) = Ft - \frac{F}{2}\left(\frac{a^2}{\alpha} + \frac{H}{\pi k}\right)\ln\left(\frac{r}{b}\right) - \frac{F(b^2 - r^2)}{4\alpha} \tag{12}$$

Replacing $\alpha$ with $k/C$ in equation (12) leads to:

$$T(r,t) = Ft - \frac{F}{2}\left(\frac{a^2 C}{k} + \frac{H}{\pi k}\right)\ln\left(\frac{r}{b}\right) - \frac{F(b^2 - r^2)C}{4k}$$

$$T(r,t) = F\left\{t - \frac{1}{4\pi k}\left[(2\pi a^2 C + 2H)\ln\left(\frac{r}{b}\right) + \pi(b^2 - r^2)C\right]\right\} \tag{13}$$

where $C \equiv C_{specimen}$.

The temperature difference across the specimen, $\Delta T$, is given by:

$$\Delta T = T(b,t) - T(a,t) = \frac{F}{4\pi k}\left[(2\pi a^2 C + 2H)\ln\left(\frac{a}{b}\right) + \pi(b^2 - a^2)C\right] \tag{14}$$

Collecting together the terms involving $C$,

$$\Delta T = \frac{F}{4\pi k}\left\{2H\ln\left(\frac{a}{b}\right) + \left[\pi(b^2 - a^2) + 2\pi a^2\ln\left(\frac{a}{b}\right)\right]C\right\} \tag{15}$$

Simply moving the $k$ and $\Delta T$ from one side of the expression to the other gives as a final result:

$$k = \frac{F}{4\pi\Delta T}\left\{2H\ln(\frac{a}{b}) + \left[\pi(b^2 - a^2) + 2\pi a^2\ln(\frac{a}{b})\right]C\right\} \tag{16}$$

Substituting for $H$ and $C$ in terms of densities and heat capacities gives:

$$k = \frac{F}{4\pi\Delta T}\left\{2\pi a^2\rho_{slug}c_p^{slug}\ln\left(\frac{a}{b}\right) + \left[\pi(b^2 - a^2) + 2\pi a^2\ln\left(\frac{a}{b}\right)\right]\rho_{FRM}c_p^{FRM}\right\} \tag{17}$$

where $c_p$ is the heat capacity in J/(kg·K).

If the masses of the slug, $M_{slug}$, and FRM specimen, $M_{FRM}$, are known and the steel rod has a height of $h$ in meters, one has:

$$k = \frac{F}{4\pi\Delta T}\left\{2\frac{M_{slug}}{h}c_p^{slug}\ln\left(\frac{a}{b}\right) + \left[1 + 2\frac{a^2}{(b^2 - a^2)}\ln\left(\frac{a}{b}\right)\right]\frac{M_{FRM}}{h}c_p^{FRM}\right\} \tag{18}.$$

For a rectangular geometry and one-dimensional heat transfer, the thermal conductivity is given by the following expression [4,5]:

$$k = \frac{Fl\left(M_{slug}c_p^{slug} + M_{FRM}c_p^{FRM}\right)}{2A\Delta T} \tag{19}$$

where
$l$ = the FRM specimen thickness, m, and
$A$ = the FRM specimen area, $m^2$.

For either geometry, if the dimensions, masses, and heat capacities of the steel slug and FRM as a function of temperature are known, the thermal conductivity as a function of mean FRM specimen temperature can be calculated using either equation (18) or (19), by measuring the temperature difference across the FRM specimen and the rate of change in the slug temperature ($F$), as detailed in the ASTM E-2584-07 standard practice [8]. In typical use [8], the heat capacity of steel as a function of temperature is employed in equations (18) and (19), while that of the FRM may be assumed to be equivalent to its room temperature value if that is the only measurement that is readily available. Measured mass loss from the specimen is distributed uniformly with mean specimen temperature during the first heating cycle [4,6]. To avoid the confounding influences of reactions, phase changes, and mass transport occurring during the first heating cycle of the slug calorimeter test, typically, the data generated during a subsequent second heating/cooling cycle is utilized to calculate the (apparent) thermal conductivity of the specimen. Still, comparing the first and second heating cycles provides valuable information on the extent of these confounding influences [4,6-8].

## Adhesion

The adhesion properties of an FRM are equally important as its thermophysical properties. Specifically, the materials must provide sufficient adhesion to structural steel so that they remain in place during a real world fire exposure. Currently, adhesion properties of FRM to steel are evaluated in the field using the ASTM E736-00(2006) standard test method [9], commonly referred to as the "mayonnaise cap" test. Recently, efforts at NIST have focused on developing materials science-based laboratory and field test methods for quantifying adhesion [10]. Using a fracture mechanics approach, the adhesion of the spray-applied FRM (SFRM)/steel assembly in "peeling" mode can be characterized by the fracture energy, $G_C$. Fig. 2 illustrates schematically a single cantilever beam (SCB) configuration. A generic equation for calculating $G_C$ in an elastically strained body (such as that in Fig. 2) is given by:

$$G_C = \frac{P^2}{2b}\frac{dC}{da} \tag{20}$$

where $P$ is the load, $a$ is the crack length, $b$ is the width of the specimen, and $C$ is the compliance (i.e. displacement/load). The SCB configuration in Fig. 2 can be modeled as a beam on an elastic foundation [11], where the governing equation from beam theory is given by:

$$\frac{d^4u}{dx^4}+4\lambda^4 uH(x)=0 \quad \text{with} \quad \lambda=\left(\frac{K}{4E_{steel}I_{steel}}\right)^{\frac{1}{4}} \qquad H(x)=\begin{cases}1, & x>0\\ 0, & x<0\end{cases} \tag{21}$$

where $E_{steel}$ and $I_{steel}$ are the Young's modulus and second moment of inertia for the beam, respectively, $u$ is the deflection of the beam, and $K$ is the stiffness of the foundation. The assumptions of the beam on elastic foundation model include: 1) linear-elastic behavior; 2) shear deformations are negligible; 3) plane cross sections remain planar and normal to the beam axis during the deformation; and 4) the curvature of the beam is small.

The boundary conditions are that the shear force and the moment at the unloading end ($x = c$) are both zero, while those at the loading point ($x = –a$) are equal to $P$ and zero, respectively. Using these conditions and solving Equation (21) gives the displacement of the beam as:

$$u(x)=\frac{6P}{E_{steel}bh_{steel}^3\lambda^3}\left(\frac{\lambda^3x^3}{3}+a\lambda^3x^2-A\lambda x+B\right), \qquad -a\le x\le 0 \tag{22}$$

$$u(x)=\frac{6P}{E_{steel}bh_{steel}^3\lambda^3}\left[a\lambda\sin\lambda x\sinh\lambda x-\left(\frac{A-1}{2}\right)\sin\lambda x\cosh\lambda x+B\cos\lambda x\cosh\lambda x-\left(\frac{A+1}{2}\right)\cos\lambda x\sinh\lambda x\right], \qquad 0\le x\le c$$

where

$$A=\left(\frac{\sinh^2\lambda c+\sin^2\lambda c}{\sinh^2\lambda c-\sin^2\lambda c}\right)+2a\lambda\left(\frac{\sinh\lambda c\cosh\lambda c+\sin\lambda c\cos\lambda c}{\sinh^2\lambda c-\sin^2\lambda c}\right),$$

$$B=\left(\frac{\sinh\lambda c\cosh\lambda c-\sin\lambda c\cos\lambda c}{\sinh^2\lambda c-\sin^2\lambda c}\right)+a\lambda\left(\frac{\sinh^2\lambda c+\sin^2\lambda c}{\sinh^2\lambda c-\sin^2\lambda c}\right)$$

and $h_{steel}$ is the thickness of the beam. Analytically, the stiffness of the foundation, $K$, can be estimated by Hooke's law as:

$$K=\frac{E_{SFRM}b}{h_{SFRM}} \tag{23}$$

where $E_{SFRM}$ and $h_{SFRM}$ are the Young's modulus and thickness of the SFRM, respectively. By combining Equations (22) and (23) and for $c > 2h_{steel}$ (our case), the adhesive fracture energy can then be calculated from Equation (20) as:

$$G_C=\frac{6P^2(\lambda a+1)^2}{E_{steel}b^2\lambda^2h_{steel}^3} \quad \text{where} \quad \lambda=\left(\frac{3E_{SFRM}}{E_{steel}h_{SFRM}h_{steel}^3}\right)^{\frac{1}{4}} \tag{24}$$

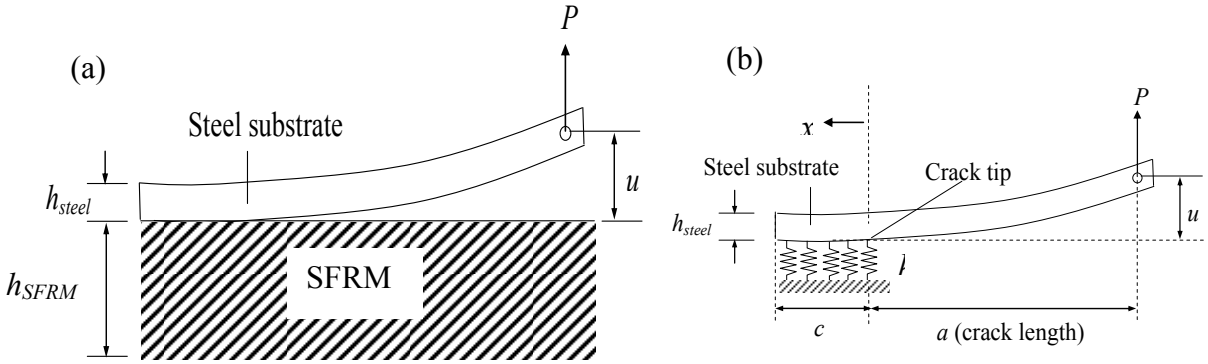


Fig 2. (a) Illustration of a single-arm cantilever beam, and (b) beam on elastic foundation (not to scale).

A typical load-displacement curve measured during such adhesion testing is shown in Fig. 3. For a set of five different FRMs that have been evaluated to date, the computed fracture energy values ranged between 0.5 J/m$^2$ and 6.5 J/m$^2$, indicating over a factor of ten difference in performance. Ongoing efforts are focused on drafting a standard test method to implement this laboratory protocol and also on developing an equivalent fracture energy-based test method for field usage. From that point, testing will then proceed to consider adhesion at high temperatures, as preliminary furnace testing has indicated significant decreases in adhesion during high temperature exposures for a variety of FRMs.

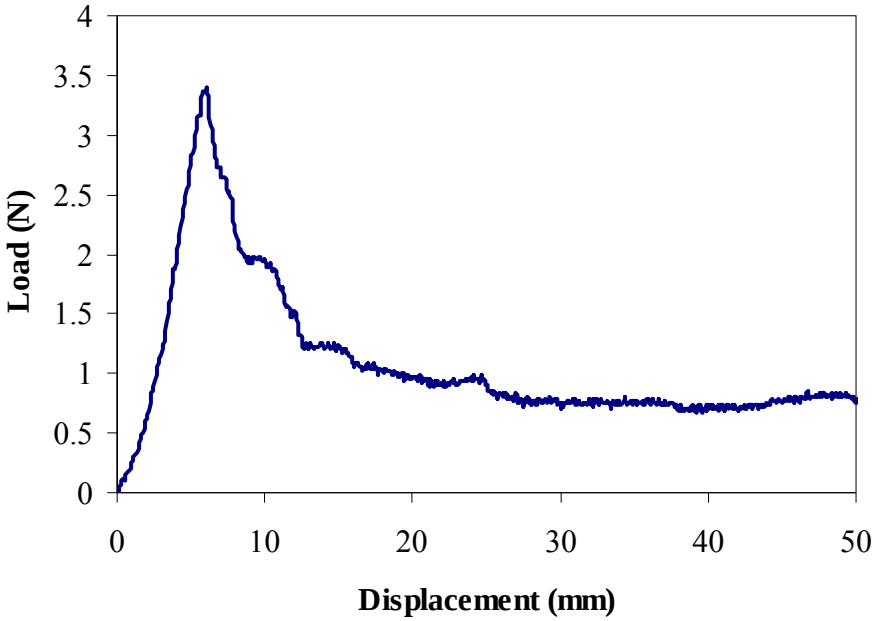


Fig 3. A typical load-displacement plot for a steel/SFRM joint. Typical crack velocity was 0.4 mm/s.

**Microstructure Characterization**

It is well established that the microstructure of porous materials has a large influence on their thermal conductivity [12-14]. FRMs may exhibit large differences in porosity (density), pore size, and pore connectivity. Intumescent coatings provide a vivid example of this as they effectively transform from a "nonporous" thin coating into a thick porous char during exposure to a fire. Recently, it has been demonstrated that the three-dimensional pore structures of FRMs can be captured using three-dimensional x-ray microtomography [14]. A captured three-dimensional microstructure can then be segmented into pores and solids and computational (finite element or finite difference) algorithms employed to compute the thermal conductivities of the FRM as a function of temperature, provided that the thermal conductivities of the porous and solid components are known (also as a function of temperature). This computational approach has been demonstrated previously for three different conventional SFRMs [14].

As an example of the capabilities of the x-ray microtomography approach, Fig. 4 provides a set of isometric two-dimensional slices from a three-dimensional dataset obtained for an intumescent coating applied to a thin-walled aluminum tube and subsequently heated to 400 ºC in a furnace. Aluminum tubes are the preferred substrate for these experiments with intumescent coatings as they absorb far fewer x-rays than steel, while still maintaining their structural integrity at the temperatures at which the charring and expansion of the intumescent is essentially complete. For the material shown in Fig. 4, the char actually had sufficient structural integrity that the aluminum tube could be "cored out" of the specimen using a simple cork bore of a slightly larger diameter, prior to imaging the specimen in the microtomography equipment; removal of the aluminum tube increases the transmission of x-rays through the "specimen". The

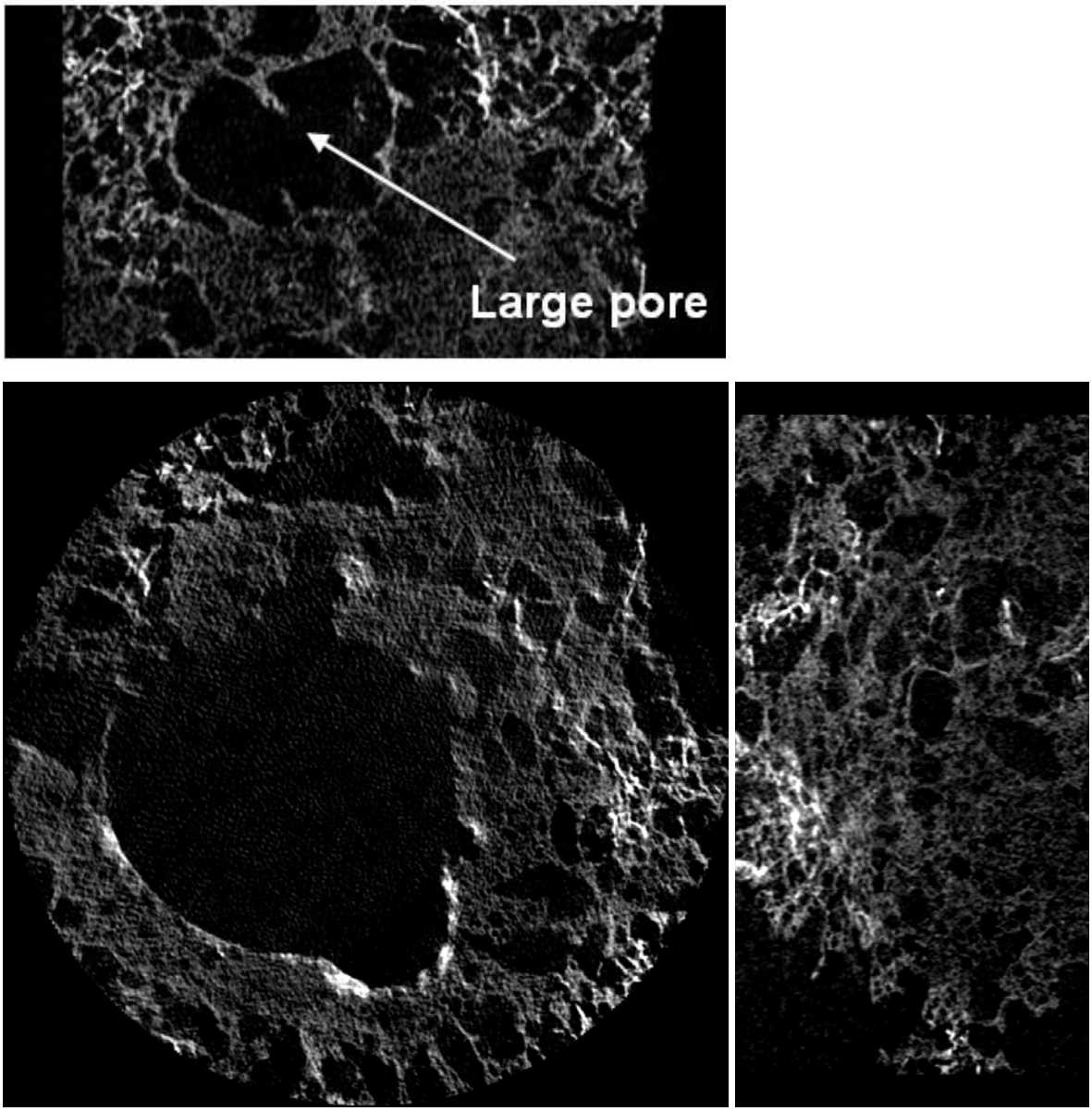


Fig. 4. Coronal (top left), transaxial (bottom left), and sagittal (bottom right) views of a cylindrical specimen (core) of an expanded intumescent coating. Transaxial image is 33 mm by 33 mm in size. The large central hole in the transaxial image was produced by the coring process and is not a void in the intumescent coating, while the large irregular pore in the coronal image is a true void within the expanded intumescent FRM.

three-dimensional pore structure of the expanded intumescent is quite complex, containing a wide variety of pore sizes and shapes, some more than five millimeters in size. Since radiative heat transfer scales directly as the pore size, these larger size pores will contribute to increased heat transfer, especially at higher temperatures where radiation is dominant over conduction, and could thus reduce the insulative effectiveness of the intumescent FRM. These images clearly demonstrate the potential of using x-ray microtomography as a research and development tool for facilitating the production of intumescent coatings with superior thermal barrier properties.

## Summary and Prospectus

Ongoing efforts to develop new materials science-based test methods for the thermophysical and adhesion properties of FRMs have been presented. A new test method for apparent thermal conductivity at high temperatures, based on the use of a slug calorimeter, has been standardized and is currently the subject of an ASTM interlaboratory study to establish a multi-laboratory precision statement. In this paper, a new analytical solution for the slug calorimeter for the case of a cylindrical (pipe) geometry has been presented. New test methods for the adhesion properties of SFRMs are also being developed, employing a fracture mechanics-based approach. Both laboratory and field test methods are envisioned; these test procedures will also be modified in the future to provide critical information on high temperature adhesion properties. Finally, it has been demonstrated that x-ray microtomography can be a valuable tool for providing actual three-dimensional images of the (internal) microstructure of SFRMs. This technique will be particularly valuable to the development and optimization of intumescent formulations, where the foaming/charring process and the resultant pore size distribution will have a strong influence on the insulative properties and performance of the expanded intumescent coating.

In the future, the properties provided by these test methods will be employed not only for comparison and evaluation purposes, but also as inputs into multi-dimensional models of the thermal and structural performance of components and systems exposed to a fire. Such models will need to employ not only the temperature-dependent property values obtained by the test methods described here, but also quantitative information on reactions, phase changes, mass transport, and substantial dimensional changes that occur to varying degrees for various FRMs at elevated temperatures.

## Acknowledgements

The authors thank the current members of the Performance Assessment and Optimization of Fire Resistive Materials consortium for their financial and technical support: the American Iron and Steel Institute, Isolatek International, PPG Industries, Inc., and W.R. Grace & Co.-Conn.

## References


[1] NIST NCSTAR 1: Federal Building and Fire Safety Investigation of the World Trade Center Disaster: Final Report on the Collapse of the World Trade Center Towers, U.S. Department of Commerce, September 2005.

[2] Bentz, D.P., Prasad, K., and Yang, J., "Towards a Methodology for the Characterization of Fire Protection Materials with Respect to Thermal Performance Models," Fire Mater., Vol. 30, No. 4, 2006, pp. 311-321.

[3] Bentz, D.P., and Prasad, K., "Thermal Performance of Fire Resistive Materials I. Characterization with Respect to Thermal Performance Models," NISTIR **7401**, U.S. Department of Commerce, February 2007.

[4] Bentz, D.P., "Combination of Transient Plane Source and Slug Calorimeter Measurements to Estimate the Thermal Properties of Fire Resistive Materials," J. Test. Eval., Vol. 35, 2007, pp. 240-244.

[5] Fitch, A.L., "A New Thermal Conductivity Apparatus," Am. Phys. Teach., Vol. 3, 1935, pp. 135-136.

[6] Bentz, D.P., Flynn, D.R., Kim, J.H., and Zarr, R.R., "A Slug Calorimeter for Evaluating the Thermal Performance of Fire Resistive Materials," Fire Mater., Vol. 30, No. 4, 2006, pp. 257-270.

[7] Do, C.T., Bentz, D.P., and Stutzman, P.E., "Microstructure and Thermal Conductivity of Hydrated Calcium Silicate Board Materials," J. Building Phys., Vol. 31, No. 1, 2007, pp. 55-67.

[8] ASTM Standard E2584-07(2007): Standard Practice for Thermal Conductivity of Materials Using a Thermal Capacitance (Slug) Calorimeter, *Annual Book of ASTM Standards*, ASTM International, West Conshohocken, PA, 2007.

[9] ASTM Standard E736-00(2006): Standard Test Method for Cohesion/Adhesion of Sprayed Fire-Resistive Materials Applied to Structural Members, *Annual Book of ASTM Standards*, ASTM International, West Conshohocken, PA, 2006.

[10] White, C.C., Tan, K.T., and Hunston, D.L., "Adhesion Test Method for Sprayed Applied Fire Resistive Materials," Proceedings of the European Adhesion Conference, 2008.

[11] Kanninen, M.F., "Augmented Double Cantilever Beam Model for Studying Crack Propagation and Arrest," Int. J. Frac., Vol. 9, 1973, pp. 83-92.

[12] Russell, H.W., "Principles of Heat Flow in Porous Insulators," J. Am. Ceram. Soc., Vol. 18, 1935, pp.1-5.

[13] Loeb, A.L., "Thermal Conductivity: VIII, A Theory of Thermal Conductivity of Porous Materials," J. Am. Ceram. Soc., Vol. 37, 1954, pp. 96-99.

[14] Bentz, D.P., Halleck, P.M., Clarke, M.N., Garboczi, E.J., and Grader, A.S., "Microstructure and Materials Science of Fire Resistive Materials," Proceedings of the ASCE/SEI Spring 2005 Structures Congress, New York, CD-RoM, 2005, available at http://ciks.cbt.nist.gov/~garbocz/ASCE_SEI (access verified October 2008).